Supplementary Information for

Modulation of electronic liquid crystal phases by local strain in few-layer FeSe films

Xuesong Gai[1,2,3], Hao Xu[1,2,3], Yi Yang[1,2,3], Yifan Guo[1,2,3], Xinyue Wang[1,2,3], Ming-Liang Zhu[4], Peng Deng[1], Haicheng Lin[1], Kai Chang[1]✉ & Chong Liu[1]✉

[1] Beijing Key Laboratory of Fault-Tolerant Quantum Computing, Beijing Academy of Quantum Information Sciences, Beijing 100193, China

[2] Beijing National Laboratory for Condensed Matter Physics, Institute of Physics, Chinese Academy of Sciences, Beijing 100190, China

[3] University of Chinese Academy of Sciences, Beijing 100049, China

[4] Key Laboratory of Pressure Systems and Safety, Ministry of Education; School of Mechanical and Power Engineering, East China University of Science and Technology, Shanghai 200237, China

✉e-mail: changkai@baqis.ac.cn; liuchong@baqis.ac.cn

Supplementary Note 1: Geometric phase analysis (GPA) for strain distribution

The geometric phase analysis (GPA) method, fully developed and documented in the 1990s[1-3], has been widely applied to high-resolution electron microscope[4,5] and STM[6,7] images for obtaining displacement and strain fields. It consists of a sequence of data calculation and conversion, outlined as follows (also see Supplementary Fig. 2).

The image intensity of a perfect lattice, as a function of the position $\boldsymbol{r}$, can be written as a Fourier series $\sum_g A_g e^{i\boldsymbol{g}\cdot\boldsymbol{r}}$, which is the sum of plane waves with different wave vectors $\boldsymbol{g}$. A_g is the intensity of each wave component. For a realistic experimental image, where both the intensity and position exhibit local deviations from the perfect lattice, the intensity map is modified as

$$T(\boldsymbol{r}) = \sum_g A_g(\boldsymbol{r}) e^{i\boldsymbol{g}\cdot(\boldsymbol{r}-\boldsymbol{u}(\boldsymbol{r}))} = \sum_g A_g(\boldsymbol{r}) e^{-i\boldsymbol{g}\cdot\boldsymbol{u}(\boldsymbol{r})} e^{i\boldsymbol{g}\cdot\boldsymbol{r}} = \sum_g A_g(\boldsymbol{r}) e^{iP_g(\boldsymbol{r})} e^{i\boldsymbol{g}\cdot\boldsymbol{r}},$$

where $P_g(\boldsymbol{r}) = -\boldsymbol{g} \cdot \boldsymbol{u}(\boldsymbol{r})$ is the phase shift due to the distortion. The vector $\boldsymbol{g}$ is taken from the Bragg peak in the Fourier transform of the image, corresponding to the reciprocal lattice vector. Using the 2D lock-in technique[1,8,9], the complex Fourier coefficient for a specific $\boldsymbol{g}$ is obtained by multiplying the image with a reference wave and applying a low-pass filter (e.g., convolution with a Gaussian function)

$$A_g(\boldsymbol{r})e^{iP_g(\boldsymbol{r})} = \int T(\boldsymbol{r}')e^{-i\boldsymbol{g}\cdot\boldsymbol{r}'}e^{-\frac{(\mathbf{r}'-\mathbf{r})^2}{2L^2}}\mathrm{d}\boldsymbol{r}'.$$

Here, L represents the averaging radius of the filter window, typically a few times the lattice period.

By carrying out the above calculations for two independent wave vectors, g_1 and g_2, one can extract the phase component images P_{g1} and P_{g2}, which contain the information of the displacement field $\boldsymbol{u}(\boldsymbol{r})$:

$$\begin{pmatrix} P_{g1} \\ P_{g2} \end{pmatrix} = -\begin{pmatrix} g_{1x} & g_{1y} \\ g_{2x} & g_{2y} \end{pmatrix}\begin{pmatrix} u_x \\ u_y \end{pmatrix}.$$

Hence, the displacement field is calculated by taking the inverse of the matrix:

$$\begin{pmatrix} u_x \\ u_y \end{pmatrix} = -\begin{pmatrix} g_{1x} & g_{1y} \\ g_{2x} & g_{2y} \end{pmatrix}^{-1}\begin{pmatrix} P_{g1} \\ P_{g2} \end{pmatrix}.$$

Here, x and y are the coordinate axes of the image (normally along vertical and horizontal directions in our algorithm). The process to this point is also referred to as Lawler-Fujita algorithm in literature for STM studies[6,10].

Then the local distortion, $e(\boldsymbol{r})$, is given by the gradient:

$$e = \begin{pmatrix} e_{xx} & e_{xy} \\ e_{yx} & e_{yy} \end{pmatrix} = \begin{pmatrix} \frac{\partial u_x}{\partial x} & \frac{\partial u_x}{\partial y} \\ \frac{\partial u_y}{\partial x} & \frac{\partial u_y}{\partial y} \end{pmatrix} = -\begin{pmatrix} g_{1x} & g_{1y} \\ g_{2x} & g_{2y} \end{pmatrix}^{-1}\begin{pmatrix} \frac{\partial P_{g1}}{\partial x} & \frac{\partial P_{g1}}{\partial y} \\ \frac{\partial P_{g2}}{\partial x} & \frac{\partial P_{g2}}{\partial y} \end{pmatrix}.$$

This matrix is further separated into a symmetric term ε and an antisymmetric term ω:

$$\varepsilon = \begin{pmatrix} \varepsilon_{xx} & \varepsilon_{xy} \\ \varepsilon_{yx} & \varepsilon_{yy} \end{pmatrix} = \frac{1}{2}(e + e^{\mathrm{T}})$$

$$\omega = \begin{pmatrix} 0 & \omega_{xy} \\ \omega_{yx} & 0 \end{pmatrix} = \frac{1}{2}(e - e^{\mathrm{T}})$$

For small distortion, ε is the strain tensor and ω is the local rotation. ε_{xx}, ε_{xx} are stretching and $\varepsilon_{xy} = \varepsilon_{yx}$ is shear strain. Lastly, a rotation transformation can be applied to ε to have the tensor represented in desired coordinates.

In addition to the lattice displacement field, a practical STM image usually contains an artifact drift field due to piezo relaxation/hysteresis, typically manifested as a nonlinear background most pronounced at the beginning of both fast- and slow-scanning directions. This can be largely removed by subtracting a cubic background from the displacement field or the distortion field during process of the aforementioned operation[6].

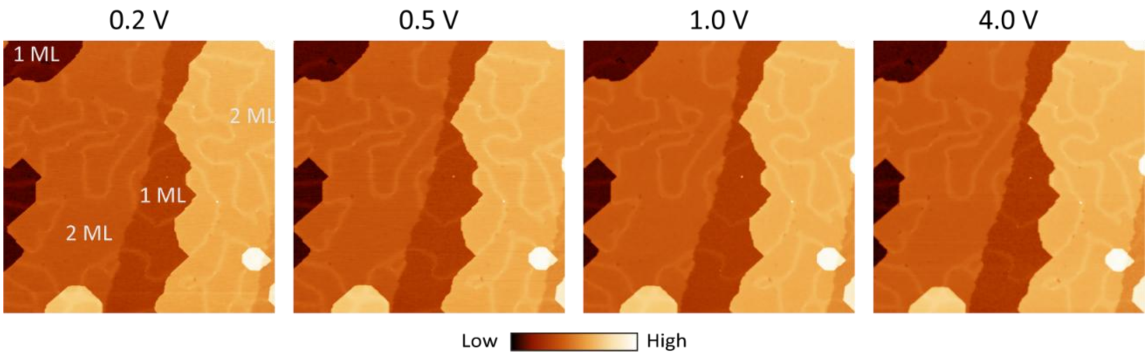

Supplementary Fig. 1 Bias-independent topography of dislocation lines. a-d STM images taken on the same area (250 nm × 250 nm) of FeSe film with various sample bias (V_s = 0.2, 0.5, 1.0 and 4.0 V. I_t = 100 pA).

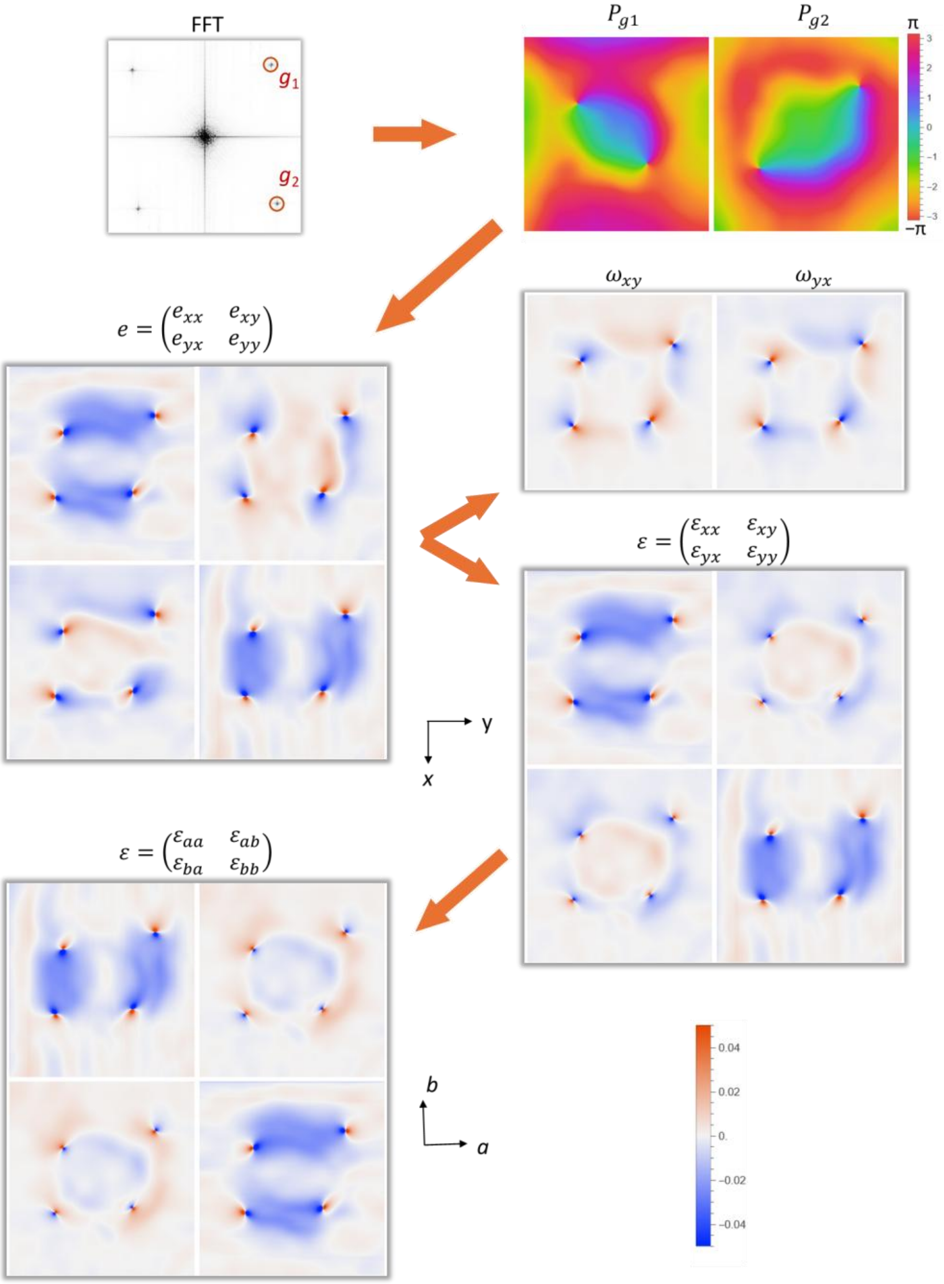

Supplementary Fig. 2 Process of the GPA on the STM image in Fig 2a. This figure demonstrates the key steps in the workflow described in Supplementary Note 1.

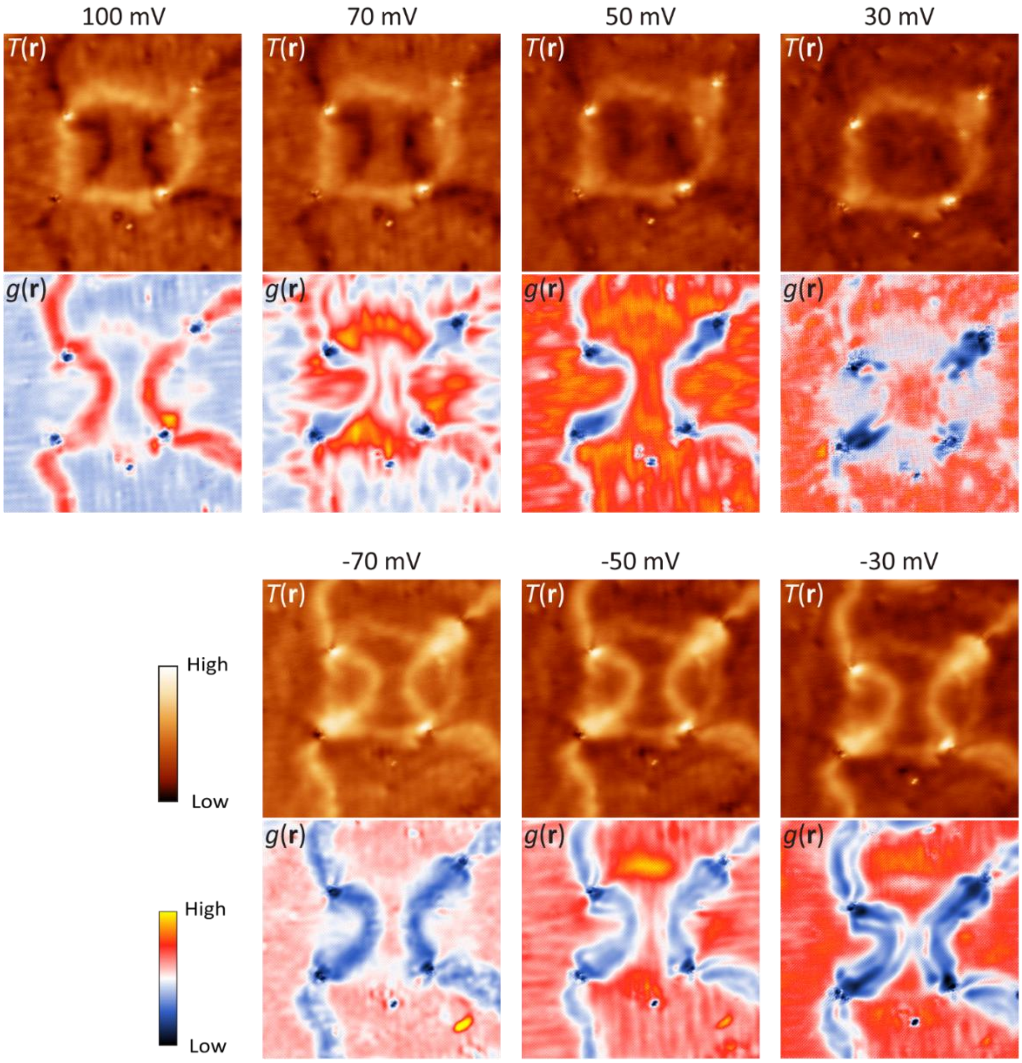

Supplementary Fig. 3 Bias-dependent intensity contrast of smectic stripes and domain walls on 2 ML FeSe. a-g Upper panels: topographic images. Bottom panels: d*I*/d*V* maps $g(\boldsymbol{r})$ of the corresponding area. (40 nm × 40 nm; $I_t = 500$ pA).

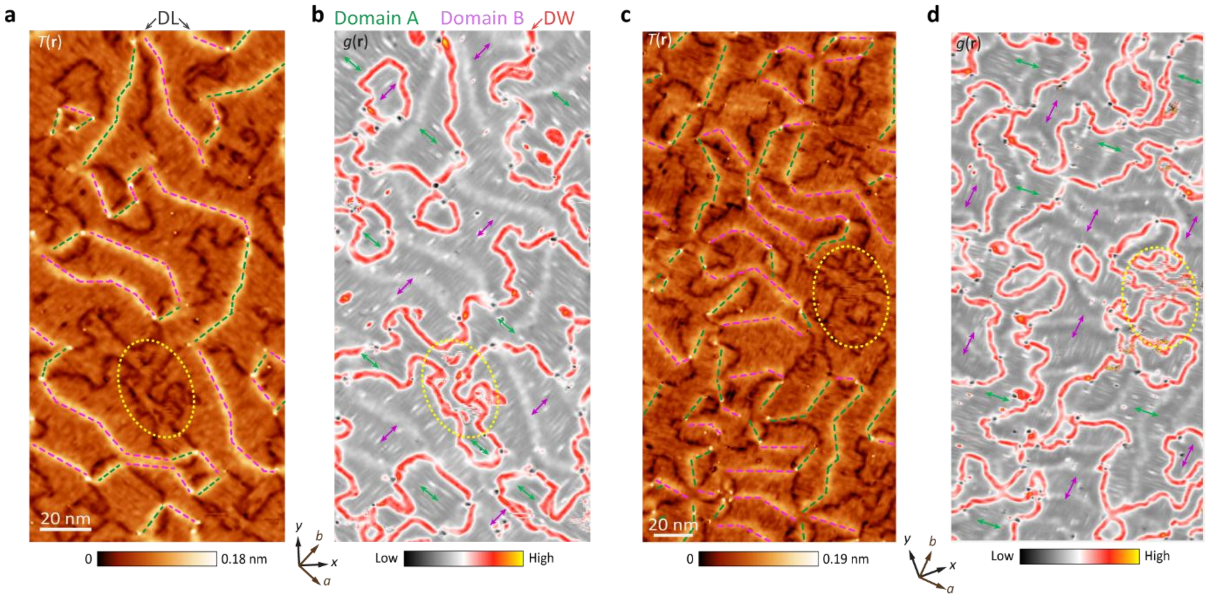

Supplementary Fig. 4 Additional large-area images taken on 2 ML FeSe for the statistical analysis in Fig. 3e. a, c STM topographic images $T(\boldsymbol{r})$ of two large areas on 2-ML FeSe. **b, d** dI/dV maps $g(\boldsymbol{r})$ of the same area in **a** and **c**, respectively. The green (magenta) double-headed arrows represent the direction of the smectic long-range stripes in domain A (B). The green (magenta) dashed lines represent the dislocation lines located in the smectic domain A (B) areas. The yellow dashed ellipses mark the areas that are away from the DLs and exhibit more fragmented domains. Scanning parameters: **a,b** 100 nm × 200 nm, V_s = 100 mV, I_t = 200 pA; **c,d** 130 nm × 260 nm, V_s = 100 mV, I_t = 500 pA.

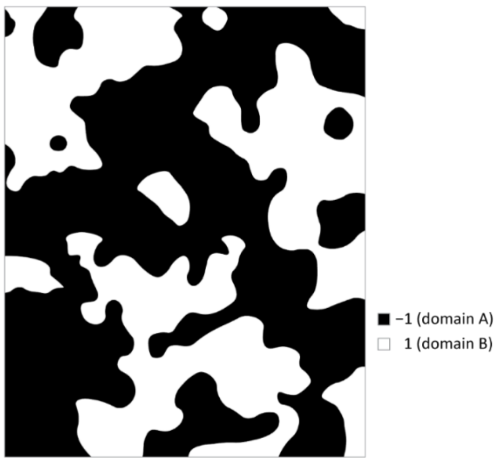

Supplementary Fig. 5 Smectic domain map corresponding to Fig. 3b. Domain walls are determined from Fig. 3b, and domains A and B are assigned with value −1 and 1, respectively. This is used for cross-correlation with Fig. 3g to yield Figs. 3h-i.

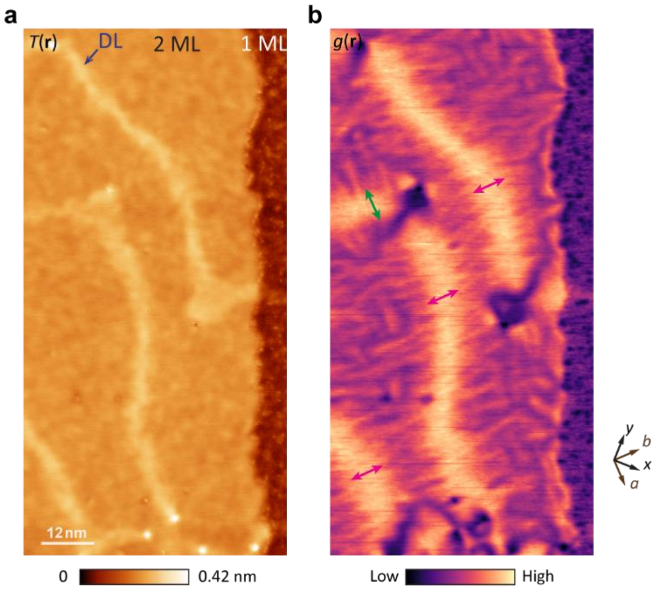

Supplementary Fig. 6 Smectic domains on 2 ML FeSe at 77 K. a STM topographic image $T(\boldsymbol{r})$, and **b** dI/dV map $g(\boldsymbol{r})$ (60 nm × 120 nm; setpoint: V_s = 50 mV, I_t = 100 pA; lock-in: 963.2 Hz, 10 mV) taken at 77 K. Large smectic domains persist near the DLs, while the domains in the other regions are so fragmented that long-range periodicity can hardly exists.

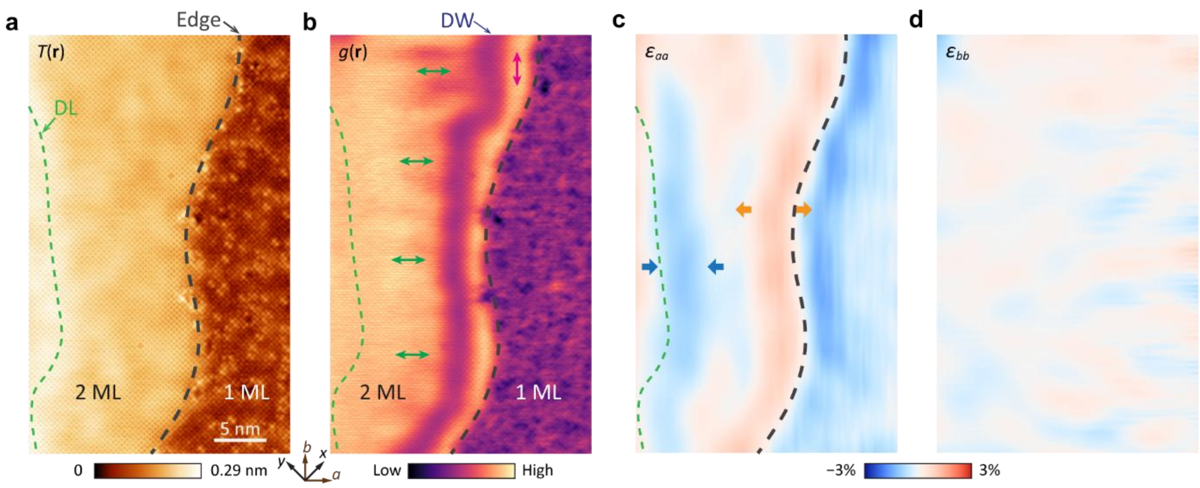

Supplementary Fig. 7 Smectic domains near a 1-2 ML step-flow edge at 77 K. a STM topographic image $T(\boldsymbol{r})$, and **b** dI/dV map $g(\boldsymbol{r})$ around the edge (25 nm × 40 nm; setpoint: V_s = 50 mV, I_t = 200 pA; lock-in: 958.9 Hz, 10 mV) at 77 K. The gray and green dashed lines mark the 1–2 ML step edge and the DL on the 2 ML, respectively. **c,d** Maps of strain tensor components ε_{aa} and ε_{bb}, which are extracted from **a** by GPA. The blue and orange arrows in **c** highlight the compressive and tensile strain along a direction, respectively, on the left and right side of the domain wall. Smectic stripes along a direction are apparent on the left, marked by green double arrows. Although the smectic stripes are not distinctly visible in the right region, the characteristic perpendicular orientation of stripes on either side of a smectic domain wall allow us to infer the presence of stripes parallel to the step at the edge.

Supplementary References

1. Takeda, M. & Suzuki, J. Crystallographic heterodyne phase detection for highly sensitive lattice-distortion measurements. *J. Opt. Soc. Am. A* **13**, 1495 (1996).
2. Hÿtch, M. J. Analysis of Variations in Structure from High Resolution Electron Microscope Images by Combining Real Space and Fourier Space Information. *Microsc. Microanal. Microstruct.* **8**, 41-57 (1997).
3. Hÿtch, M. J., Snoeck, E. & Kilaas, R. Quantitative measurement of displacement and strain fields from HREM micrographs. *Ultramicroscopy* **74**, 131-146 (1998).
4. Hÿtch, M. J., Putaux, J.-L. & Pénisson, J.-M. Measurement of the displacement field of dislocations to 0.03 Å by electron microscopy. *Nature* **423**, 270-273 (2003).
5. Zhu, Y., Ophus, C., Ciston, J. & Wang, H. Interface lattice displacement measurement to 1pm by geometric phase analysis on aberration-corrected HAADF STEM images. *Acta Materialia* **61**, 5646-5663 (2013).
6. Gao, S. *et al.* Atomic-scale strain manipulation of a charge density wave. *Proc. Natl. Acad. Sci. U.S.A.* **115**, 6986-6990 (2018).
7. Ren, Z. *et al.* Nanoscale decoupling of electronic nematicity and structural anisotropy in FeSe thin films. *Nat. Commun.* **12**, 10 (2021).
8. Du, Z. *et al.* Imaging the energy gap modulations of the cuprate pair-density-wave state. *Nature* **580**, 65-70 (2020).
9. Zeljkovic, I. *et al.* Scanning tunnelling microscopy imaging of symmetry-breaking structural distortion in the bismuth-based cuprate superconductors. *Nat. Mater.* **11**, 585-589 (2012).
10. Lawler, M. J. *et al.* Intra-unit-cell electronic nematicity of the high-T_c copper-oxide pseudogap states. *Nature* **466**, 347-351 (2010).